Enhanced On-Wafer Time-Domain Waveform Measurement Through Removal of Interconnect Dispersion and Measurement Instrument Jitter

Jonathan Brereton Scott, *Senior Member, IEEE*, Jan Verspecht, Babak Behnia, *Member, IEEE*, Marc Vanden Bossche, *Member, IEEE*, Alex Cognata, Frans Verbeyst, Mark L. Thorn, *Member, IEEE*, and Daniel R. Scherrer

***Abstract*—We measure output waveshape and rise time of two high-speed digital circuits on wafer using a 50-GHz prototype of a new instrument. The instrument uses vector error correction to deembed the component under test like a network analyzer, but reads out in the time domain after the fashion of an equivalent-time oscilloscope. With the calibration plane of the instrument set at the tips of the wafer probes, errors arising from dispersion in the connection hardware are removed. We show that the random jitter in the measurement system is removed without the convolution penalty usually incurred by averaging so that anomalies such as pattern-dependent jitter are exposed. The system rise time is 7 ps, compared to a system rise time of 12–13 ps for a conventional equivalent-time oscilloscope of the same bandwidth in the presence of wafer probes, bias networks, and cables.**

***Index Terms*—Microwave integrated circuits, microwave measurements, millimeter-wave measurements, pulse measurements, time-domain measurements.**

I. Introduction

MEASUREMENT of components intended for 40-Gb/s systems presents a new challenge. Circuits are microwave in nature. However, performance specifications typically are made in time-domain terms such as edge rise time. Time-domain information is most useful for designers to visualize circuit operation. No convenient relationship between the time- and frequency-domain performance criteria is available, and measurement of performance in the time domain is thwarted by phenomena such as cable dispersion and wafer-probe discontinuities. The eye of a 40-Gb/s signal can be closed significantly by a few inches of cable and a few transitions.

Here, we report on crucial time-domain performance measurements made with an instrument called a large-signal network analyzer (LSNA). This instrument is calibrated to a measurement plane just like the familiar vector network analyzer (VNA), yet it yields time–voltage data in a manner similar to an equivalent-time sampling oscilloscope. The prototype version of the instrument used in this paper has a 50-GHz bandwidth, and approximately 7-ps 20%–80% system rise time. Its performance will be compared with that of a 50-GHz equivalent-time oscilloscope.

Manuscript received April 2, 2002; revised August 19, 2002.

The authors are with the Microwave Technology Center, Agilent Technologies, Santa Rosa, CA 95404 USA (e-mail: jonathanscott@ieee.org).

Digital Object Identifier 10.1109/TMTT.2002.805169

II. LSNA Instrument

The LSNA is not a new development, but has previously been seen as a nonlinear network analyzer for device or behavioral circuit modeling [1]–[3]. Although yielding time-domain data, the instrument internally resembles a VNA or microwave transition analyzer (MTA) that would use a sinewave stimulus. However, it is equally valid to think of it as an *oscilloscope with error correction*. Viewed this way, it can be seen as an ideal tool for making precision time-domain wafer-level waveform measurements in the presence of dispersive cables, imperfect adapters, and unavoidable device probes. This is precisely the need in the case of characterization of 40-Gb/s data components such as multiplexers (MUXs), data amplifiers, and retiming circuits.

Fig. 1 depicts the block diagram of the LSNA. A practical LSNA contains relays that allow for reconnection during s-parameter, magnitude, and phase calibration phases. For ease of description, these have been left out and, in this paper, the calibration procedure will be described in principle only.

The constraints on the use of an LSNA are twofold. Firstly, any waveform to be examined must be periodic, and the period must be known. This is really the same condition that exists for equivalent-time oscilloscopes traditionally used for such measurements since these must normally be provided with a trigger signal at or below the fundamental frequency of the signal being measured.

Secondly, all frequency components present in the waveform must be anticipated. In other words, the LSNA must be calibrated at all the frequencies that might be present in the signal to be examined. A suitable analogy might be the use of a harmonic balance (HB) algorithm in a simulator. Unlike a transient algorithm as found in SPICE, the HB simulator also requires that one must specify all frequency orders of the stimulus signal. This constraint exists because the LSNA, though displaying data in the time domain, calibrates at single frequencies selected from a comb. The comb fundamental must be chosen, and wanted members of the comb identified. This is not usually

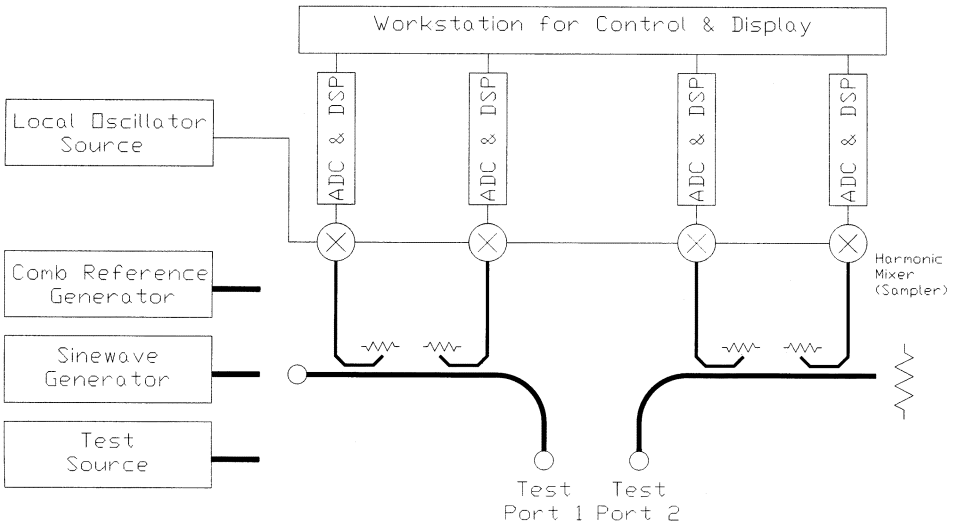

Fig. 1. Block diagram of the LSNA. Switching circuitry used during the calibration procedure has been eliminated for the interest of simplicity.

a serious constraint when testing data transmission components because both the clock rate and period of any pseudorandom bit sequence (PRBS) are known.

III. Calibrating the LSNA

The LSNA is first connected as a VNA, with a sinewave source, and a small-signal vector calibration performed at the probe tips in the customary manner. We experimentally find good accuracy using line-reflect-reflect-match (LRRM) or thru-reflect line (TRL) methods, although the TRL method requires that the probes move with respect to each other during calibration, causing complications we choose to avoid. The calibration is made at the selected fundamental and its harmonics.

Next a small-signal one-port calibration is performed at a location convenient for the attachment of connectorized components such as a power meter's sensor. This is necessary because it is impossible to connect a power sensor and harmonic phase reference to a probe tip. This calibration is carried out at the connector on the outside (non-device-under-testing (DUT) side) of the a_2 reflectometer since this does not require that the previous two-port calibration be invalidated by breaking any connections inside the couplers. The one-port calibration is carried out with a through in place of the DUT, and simple coaxial standards are used. The one-port vector calibration is followed by a power calibration carried out at the one-port calibration plane by means of attaching a power meter sensor. The VNA is now able to ratio the complex voltage waves and measure absolute power levels at the wafer-probe tips. In other words, we know not only $S_{11} = b_1/a_1$, etc., but also the absolute value of the magnitudes of a_1 and, thus, also b_1, etc.

Next, the sinewave source is disconnected and a comb reference generator is connected at the one-port (coaxial) calibration plane. Care is taken in all calibrations to have the same ultimate signal frequency reference and, thus, the same sources of stochastic jitter. This typically means that the comb generator is driven by the source previously used for the small-signal calibrations, and the LSNA local oscillator (LO) source remains locked by the same means to this original signal source. The reference generator is driven with a fundamental frequency that is a subharmonic of all the frequencies included in the small-signal calibration. The reference comb provides the absolute phase reference that allows the instrument to relate the phase (timing) of traveling-wave signals measured at different frequencies.

The corrected magnitude and phase of each harmonic component relative to a known universal subharmonic is now established at the probe tips. When performing a measurement, the LSNA uses the absolute magnitude and known relative phase (timing) of all harmonics of each traveling wave (a_1, etc.) to carry out an inverse Fourier transform to produce the time-domain waveform.

Of course, accuracy of the result relies on knowing the relative phase of all harmonics of the reference comb generator within the bandwidth of the measurement. The reference comb generator was carefully characterized via a nose-to-nose calibration [4], [5]. Improvements in the nose-to-nose calibration method are the subject of a patent application, and traceability of the reference generator magnitude and phase to 110 GHz is in the process of being established, although this was not in place at the time this paper's manuscript was prepared.

IV. Amplifier Results

We will examine the performance of two high-speed integrated circuits (ICs) tested on a wafer-probe station. The first circuit is a data amplifier that is intended to be run in a limiting mode with output of 3–3.5 V peak to peak into 50 Ω at a fundamental frequency of approximately 21 GHz. It can also be used as a clock amplifier with a fundamental frequency of approximately 43 GHz. A 4 : 1 MUX will also be evaluated. The MUX has current-mode logic (CML, 0 to -0.5 V) output into 50-Ω suitable for driving the data amplifier.

We are interested in the performance of the circuits on fast transitions, specifically such characteristics as rise time, overshoot, ringing, etc. We wish to measure the performance at the wafer pads, to provide feedback to circuit designers, and to distinguish this from performance measured when fully packaged.

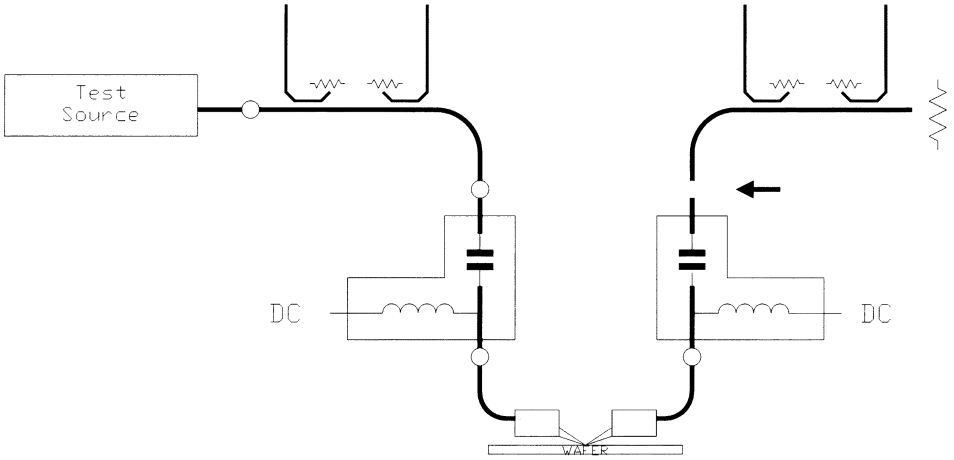

Fig. 2. Actual measurement setup used to compare the LSNA results to those obtained with direct oscilloscope tests of the data amplifier. Note that both a 50-GHz wafer probe and 50-GHz bias network are present between the measurement instrument and DUT. The arrow identifies the closest point at which a conventional sampling oscilloscope can be connected. Had we not sought to carry out a direct comparison with a sampling oscilloscope for the purpose of this paper, the bias networks could have been located outside the directional couplers.

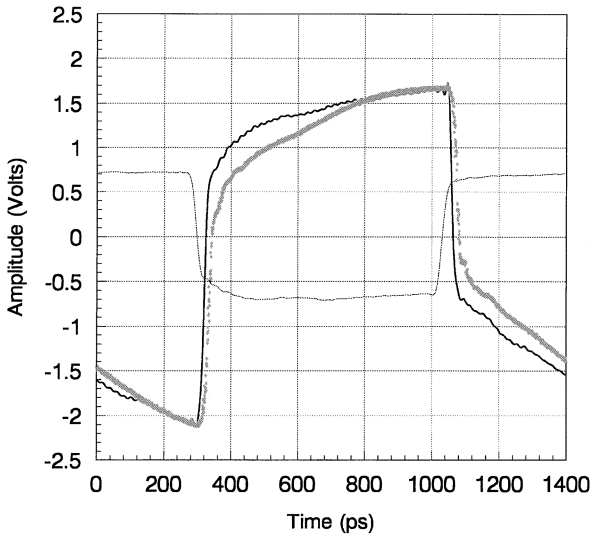

Fig. 3. Measurement results showing the amplifier output waveform obtained using the new instrument. The trace composed of dots shows a measurement carried out with a conventional sampling scope, and the reduced-amplitude inverted waveform is the input signal to the amplifier. The stimulus fundamental frequency is 700 MHz.

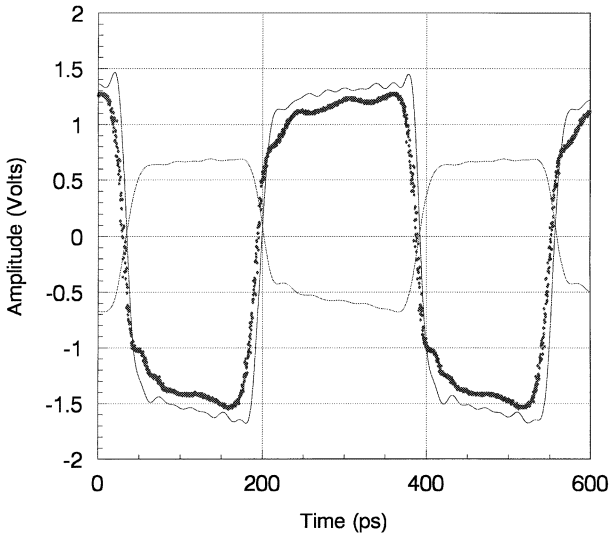

Fig. 4. Measurement results similar to those of Fig. 3, but for a fundamental stimulus at 2.8 GHz instead of 700 MHz.

Fig. 2 shows the connection used for the amplifier measurement. In the past, such a measurement would have been made with a sampling oscilloscope. The presence of the bias networks, wafer probes, and interconnection hardware such as cables and adapters, would progressively degrade system rise time. Using the LSNA, these components will be effectively removed by calibration at the probe tips.

Fig. 3 shows the measured output signal obtained from the LSNA. The same plot shows measurements of the input signal, along with the output signal obtained from a 50-GHz sampling oscilloscope. Fig. 4 shows similar results, but with a fundamental square-wave frequency of 2.8 GHz, four times higher than the signal used for Fig. 3. Fig. 5 shows an expanded view of the first rising transition of the data in Fig. 4.

V. Analysis of Amplifier Results

The LSNA yields a continuous trace, in the sense that it contains its result in "analytic" form, and can tabulate numeric output with arbitrary point density. It is also capable of analytically reporting measured slope of a transition. In contrast, the sampling oscilloscope has a prespecified point density, each sample being one measurement made in response to one trigger event. (The oscilloscope was used with no averaging.) The reported 20%–80% rise times are $\approx$11 and $\approx$15 ps, respectively, but depend a little on the end-of-transition levels selected. Peak slopes are around 130 and 90 V/ns.

With a 700-MHz fundamental, the LSNA is measuring 71 harmonics, employing almost the full 50-GHz bandwidth. A system with a bandwidth of 50 GHz, but with a rapid fall in response above 50 GHz, should theoretically have a 20%–80%

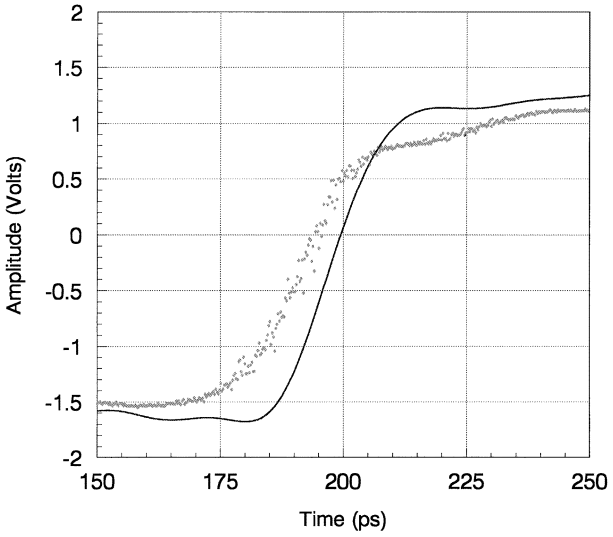

Fig. 5. LSNA and oscilloscope measurements from Fig. 4 expanded about the first rising transition. Peak slopes are around 130 and 90 V/ns.

rise time of approximately 7 ps.[1] We may approximately "deconvolve" the response of the system from the response of the device using the rule-of-thumb that rise times accumulate as the root of the sum of their squares. The LSNA reports a rise time of 11 ps, suggesting an actual waveform rise time of ≈7–8 ps.

Allowing for the bias network (5 ps), wafer probe (6 ps), adapter (4 ps), and oscilloscope response (7 ps), we might expect the oscilloscope system to represent an ideal rise time of $\sqrt{7^2+5^2+4^2+6^2}$, just over 11 ps, perhaps 1–2 ps larger to allow for some cable loss. Our comparative oscilloscope measurement, taken by breaking the circuit at the point marked with an arrow in Fig. 2, gives a rise time of 15 ps, implying a system rise time of 12–13 ps consistent with this rough estimate, as some 15 cm of cable is present. Note that while we are able to go forward through the calculation above, it would be extremely precarious to start with a rise time of 15 ps and go backward to conclude a signal rise time of 7 or 8 ps.

In Fig. 4, the oscilloscope trace shows some ringing with a frequency near 9 GHz, but the LSNA trace does not. The oscilloscope trace shows a lower amplitude, accounted for by the response of the components (wafer probe, cables, bias network) between the device and its connector. The LSNA waveform is beginning to exhibit Gibb's phenomenon, visible mainly as ringing appearing at the beginning of the transitions.

It is interesting to note that both systems exhibit misleading fine structure in the waveshape, but for different reasons. The fine structure is apt to vary with stimulus frequency content for the oscilloscope case as a consequence of its overall response not being flat. In the LSNA case, the fine structure will vary with fundamental frequency in accordance with Gibb's phenomenon and the relative position of the fundamental and the absence of any data above the highest calibration frequency.

[1]For comparison, a 50-GHz system with single-pole rolloff would exhibit a 20–80 rise time of just over 4 ps, while a system with a fifth-order rolloff—more representative of an actual oscilloscope—would exhibit around 6 ps.

VI. Jitter and Averaging

Use of averaging with a conventional sampling oscilloscope can compromise the bandwidth as a consequence of trigger jitter [6]. We now show that the so-called absolute calibration method employed in the LSNA eliminates systematic errors that would otherwise be introduced by time jitter. First, we investigate what the relationship is between the jitter probability density function and the systematic errors encountered. Assume that we apply a periodic waveform $x(t)$ with a period T_0. We can represent this signal by a set of complex Fourier series coefficients X_i, with index i going from zero to infinity. The relationship between $x(t)$ and X_i can be written

$$x(t) = \sum_{i=0}^{\infty} \Re\left(X_i e^{j2\pi i(t/T_0)}\right). \tag{1}$$

The Fourier series coefficient X_i is called the ith harmonic of the signal $x(t)$. In practice, a limited number of harmonics is sufficient to faithfully represent a signal. The LSNA allows the measurement of all harmonics X_i of $x(t)$ with frequencies below 50 GHz.

We now investigate the systematic errors caused by introducing time jitter noise. The components X_i are measured in the LSNA by sampling the signal $x(t)$ and by using a discrete Fourier transform (DFT). The jitter noise will be represented by a stochastic variable ϵ, with a probability density function $P(\epsilon)$. Consider now that we sample the waveform $x(t)$ with a sampling period T_s, calling the nth sample $x[n]$. One can then write

$$x[n] = \sum_{i=0}^{\infty} \Re\left(X_i e^{j2\pi i((nT_s+\epsilon[n])/T_0)}\right). \tag{2}$$

In (2), $\epsilon[n]$ represents the realization of the stochastic variable ϵ for the nth sample. In order to find the systematic error caused by the presence of ϵ, we will calculate the expectation of the sampled signal $x[n]$, denoted $\langle x[n]\rangle$. This is done so

$$\begin{aligned}\langle x[n]\rangle &= \int_{-\infty}^{\infty} \sum_{i=0}^{\infty} \Re\left(X_i e^{j2\pi i((nT_s+\epsilon)/T_0)}\right) P(\epsilon)\,d\epsilon \\ &= \sum_{i=0}^{\infty} \Re\left\{X_i \left(\int_{-\infty}^{\infty} e^{j2\pi i((\epsilon)/T_0)} P(\epsilon)\,d\epsilon\right) e^{j2\pi i(nT_s/T_0)}\right\}\end{aligned} \tag{3}$$

which leads to

$$\langle x[n]\rangle = \sum_{i=0}^{\infty} \Re\left\{X_i F_\epsilon\left(\frac{2\pi i}{T_0}\right) e^{j2\pi i(nT_s/T_0)}\right\} \tag{4}$$

where the function $F_\epsilon(.)$ is equal to the Fourier transform of the probability density function $P(.)$. In statistics, $F_\epsilon(.)$ is also called the characteristic function of the stochastic variable ϵ.

We interpret (4) to say that the expectation of the sampled waveform is equal to the jitter-free sampled waveform of a filtered version of $x(t)$, where $F_\epsilon(.)$, the characteristic function of ϵ, represents the frequency transfer function of the filter that is applied. However, the LSNA calibration procedure has been designed to remove the systematic errors due to *all* of the microwave hardware (using a power meter for amplitude calibra-

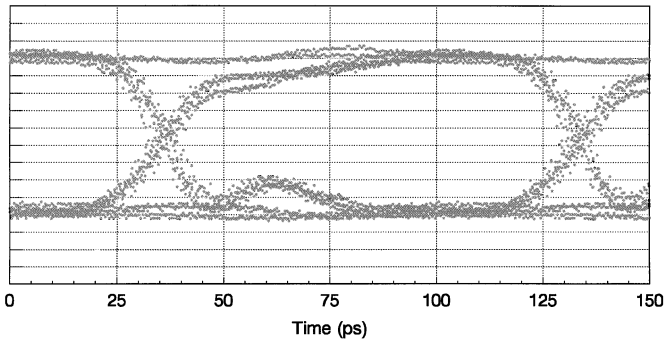

Fig. 6. Output of a MUX running at 10.24 GB/s viewed with a 50-GHz sampling scope. The data stream is a PRBS of length 16 bits.

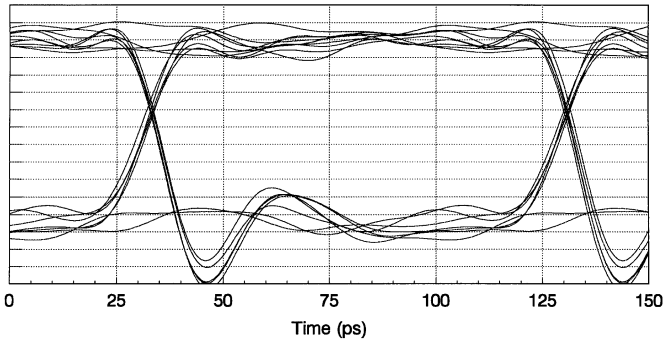

Fig. 7. Output waveform of the same MUX used for Fig. 6, but obtained using the 50-GHz LSNA prototype, with the calibration reference plane set at the IC output pad.

tion and a harmonic phase reference for phase calibration). As such, it will also eliminate this systematic error caused by the timing jitter. This can easily be understood since the systematic error caused by timing jitter manifests itself as an additional linear distortion, which cannot be distinguished from linear distortion caused by the hardware. It has been assumed that the same jitter is present during calibration as during the measurement: This condition is carefully met in normal calibration of the instrument.

The elimination of random (stochastic) jitter immediately reveals pattern-dependent (deterministic) jitter, a potential cause of intersymbol interference.

VII. MUX Measurements

Fig. 6 shows the eye of a bit pattern at the output of the MUX IC as captured by an oscilloscope, where much of the "noise" on the data is jitter. This is indicated by the greater spread of points on transitions compared to regions where the level is substantially static. Fig. 7 shows the same measurement using the LSNA. Of note in the comparison of these two figures is the transition crossover asymmetry visible in the LSNA case, but mostly hidden in the scope case. We attribute the apparent rounding or "crunching" of the transitions to cable loss based on comparison of measurements taken with a calibration plane behind a short cable run with those without the cable run. Note also the 13% difference in apparent amplitude.

Fig. 8 shows the output that is expected from detailed simulation of the MUX circuit in ADS. The simulations agree well

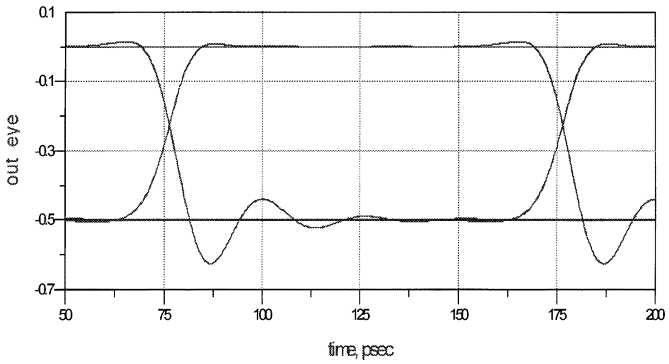

Fig. 8. Output waveform of the MUX used for Fig. 7, as simulated in ADS.

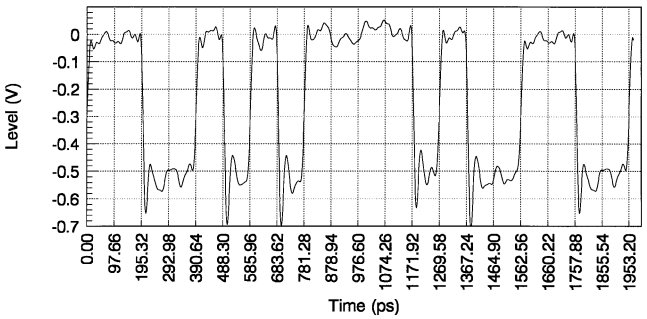

Fig. 9. MUX output waveform viewed in oscilloscope mode with the LSNA. Pattern-dependent differences in edges are evident. Some of the fine structure on bit levels can be attributed to reflections from the imperfect load presented to the device by wafer probes, adapters, etc.

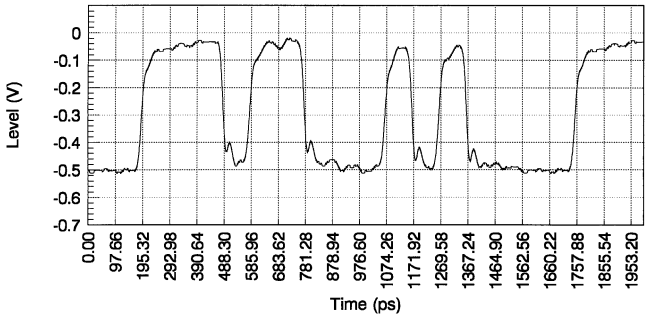

Fig. 10. MUX output waveform similar to Fig. 9, but viewed with an oscilloscope through a wafer probe, half a meter of high-quality cable, and using built-in 1024 averaging.

with the LSNA measurements, but only poorly with the scope measurements, lending further credence to the LSNA results.

Figs. 9 and 10 compare a measurement of a bit stream using the LSNA with a similar measurement on the same device using an oscilloscope with 1024 averaging. The distortion, loss of detail, and reduced amplitude resulting from dispersion and from the use of averaging in the presence of jitter are clearly visible.

VIII. Conclusions

We have shown that it is possible to make time-domain measurements independent of dispersion in the connections to a circuit, and without contributions arising from measurement system timing jitter. As a consequence of this, rise time can be measured with no interference or degradation from wafer

probes, connecting hardware, or jitter, and long connecting cables do not close the eye of a data stream. The 50-GHz prototype has a system rise time of 7 ps. A 110-GHz version could be expected to have a rise time below 3.5 ps.

REFERENCES

[1] D. Barataud, A. Mallet, M. Campovecchio, J. M. Nebus, J. P. Villotte, and J. Verspecht, "Measurements of time domain voltage/current waveforms at R.F. and microwave frequencies for the characterization of nonlinear devices," in *Proc. IEEE Instrum. Meas. Technol. Conf.*, vol. 2, May 1998, pp. 1006–1010.

[2] J. Benedikt, R. Gaddi, P. J. Tasker, M. Goss, and M. Zadeh, "High power time domain measurement system with active harmonic load-pull for high efficiency base station amplifier design," in *IEEE MTT-S Int. Microwave Symp. Dig.*, vol. 3, June 2000, pp. 1459–1462.

[3] D. Schreurs, J. Wood, N. Tufillaro, L. Barford, D. Usikov, and D. Root, "The construction and evaluation of behavioral models for microwave devices based on time-domain large-signal measurements," in *IEEE Int. Electron Devices Meeting*, San Francisco, CA, 2000, Paper 35.4, pp. 819–822.

[4] T. Van den Broeck and J. Verspecht, "Calibrated vectorial nonlinear-network analyzers," in *IEEE MTT-S Int. Microwave Symp. Dig.*, May 1994, pp. 1069–1072.

[5] J. Verspecht, "Broadband sampling oscilloscope characterization with the 'Nose-to-nose' calibration procedure: A theoretical and practical analysis," *IEEE Trans. Instrum. Meas.*, vol. 44, pp. 991–997, June 1995.

[6] ——, "Compensation of timing jitter-induced distortion of sampled waveforms," *IEEE Trans. Instrum. Meas.*, vol. 43, pp. 726–732, Oct. 1994.

[7] J. B. Scott, B. Behnia, M. Vanden Bossche, A. Cognata, J. Verspecht, F. Verbeyst, M. Thorn, and D. R. Scherrer, "Removal of cable and connector dispersion in time-domain waveform measurements on 40 Gb integrated circuits," in *IEEE MTT-S Int. Microwave Symp. Dig.*, June 2002, Paper TH2E-4, pp. 1669–1672.

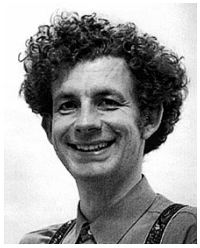

Jonathan Brereton Scott (S'90–M'97–SM'98) was born in Brisbane, Australia, in 1956. He received the B.Sc., B.E., Master of Engineering, and Ph.D. degrees from the University of Sydney, Sydney, N.S.W., Australia, in 1977, 1979, 1986, and 1997, respectively.

He was with the Air Navigation Group, a research arm of the Department of Transport, where he was involved with microwave transient digitization. He was a consultant in a variety of industries, including radar and analog signal processing. He then became Manager of the Sydney Microwave Design Resource Centre from 1988 to 1992, as well as a Senior Lecturer with the Department of Electrical Engineering, University of Sydney. He was involved in establishing and subsequently teaching in the Graduate Program in Audio, School of Architectural and Design Science. In 1995, he was a visitor with University College London, London, U.K. He subsequently became a Visiting Lecturer with the University of Western Sydney. In 1994, he was with Macquarie University, where he was involved with nonlinear electronic systems and assisted in the setup of the Collaborative Nonlinear Electronic Research Facility (CNERF) in conjunction with the Electronics Department, Macquarie University, and Macquarie Research Limited. In 1997, became Chief Engineer with RF Technology Ltd. In 1999, he joined the Microwave Technology Division, Hewlett-Packard (now Agilent Technologies), Santa Rosa, CA. He has authored over 50 refereed publications and an undergraduate textbook.

Dr. Scott is a Fellow of the Institution of Engineers, Australia. He is a member of the Audio Engineering Society (AES). He is an Honorary Associate of Macquarie University. He has served on committees of the Standards Association of Australia. He was the recipient of a 1993 British Telecom Research Fellowship and the 1994 Electrical Engineering Foundation Medal for Excellence in Teaching.

Jan Verspecht was born on December 12, 1967, in Merchtem, Belgium. He received the Electrical Engineering and Ph.D. degrees from the Vrije Universiteit Brussel (VUB), Brussels, Belgium, in 1990 and 1995, respectively.

Upon graduation in 1990, he became a Research Engineer and later a Technical Lead for the Network Measurement and Description Group (NMDG), Hewlett-Packard Company (which became a part of Agilent Technologies), Bornem, Belgium, in 1999. He is currently involved with advanced measuring and modeling techniques to deal with large-signal behavior of microwave devices.

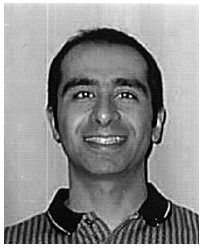

Babak Behnia (M'02) was born in Tehran, Iran, on October 7, 1971. He received the B.S. degree in electrical engineering from the University of California at Berkeley, in 1994, the M.S. degree (with a focus on RF probes for limited sample detection in nuclear magnetic resonance) and Ph.D. degree in electrical engineering from the University of Illinois at Urbana-Champaign, in 1997 and 2002, respectively. His doctoral research concerned the design of a microwave hyperthermia system integrated with an MRI system for feedback control of heating and noninvasive mapping of microwave properties of tissues.

He was a Programmer for nine months with Silicon Graphics, Mountain View, CA, prior to relocating to Champaign, IL. He is currently an IC Design Engineer with Agilent Technologies, Santa Rosa, CA. His current area of focus is generation of fast pulses using nonlinear transmission lines.

Marc Vanden Bossche (M'89) received the Electrotechnical–Mechanical Engineer degree and Ph.D. degree in electrical engineering from the Vrije Universiteit Brussel (VUB), Brussels, Belgium in 1984 and 1990, respectively.

From 1985 to 1987, he was a Research Assistant with the National Fund for Scientific Research, Brussels, Belgium. In 1987, he joined the Hewlett-Packard Company, Santa Rosa, CA. In 1991, he established a Hewlett-Packard Research and Development team in Belgium, which focuses on characterization and modeling tools for high-frequency electrical components. Currently with Agilent Technologies, he and the research team continue to develop large-signal network analysis tools for RF, microwave, and high-speed digital components.

Alex Cognata received the Associate of Science degree in electronic technology from Santa Rosa Junior College, Santa Rosa, CA, in 1983.

He is currently a Measurement System Specialist with the Microwave Technology Center, Agilent Technologies, Santa Rosa, CA. His recent interests include linear systems theory and digital signal processing (DSP). His contributions include test system hardware and software development for large-signal greybox model extraction and verification. He works on the 50-GHz LSNA and enabled measurement of vector-corrected voltage and current waveforms for the Microwave Technology Center. His previous work was on harmonic load–pull measurement. He set up and ran the load–pull measurement service, which is offered both within Agilent Technologies and to external companies.

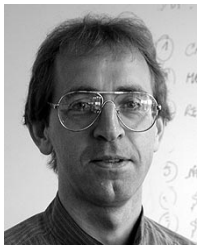

Frans Verbeyst received the Electrical Engineering degree from the Vrije Universiteit Brussel (VUB), Brussels, Belgium, in 1986, and is currently working toward the Ph.D. degree at VUB.

Since 1990, he has been with the Network Measurement and Description Group (NMDG), Agilent Technologies, Santa Rosa, CA, and is currently located in Hingene, Belgium. Since joining Agilent Technologies, he has been involved in large-signal RF and microwave measurements and behavioral modeling. He is also involved with a streamlined implementation of the "nose-to-nose" calibration procedure as an essential part of the phase calibration of LSNAs and its transfer into other groups within Agilent Technologies and into the National Institute of Standards and Technology (NIST), Boulder, CO.

Mark L. Thorn (S'76–M'79) received the B.S.E.E. (*cum laude*) and M.S.E.E. degrees from the State University of New York at Buffalo, in 1976 and 1979, respectively.

In 1979, he joined the Test and Measurement Microwave Technology Center, Hewlett-Packard Company (now Agilent Technologies), Santa Rosa, CA, where he was involved in the fabrication of discrete and integrated GaAs FET microwave components. Since then, he has held test engineering and GaAs IC product management responsibilities. He is currently a GaAs and InP Analog and Digital IC Design Engineer with the Semiconductor Research and Development Department, Agilent Technologies.

Mr. Thorn is a member of Tau Beta Pi.

Daniel R. Scherrer received the B.S., M.S., and Ph.D. degrees in electrical engineering from the University of Illinois at Urbana-Champaign, in 1991, 1993, and 1996 respectively. His doctoral research included designing low-cost high-performance millimeter-wave low-noise amplifiers (LNAs) using coplanar waveguide and ion-implanted GaAs MESFETs, as well as characterization and modeling of passive components and high-speed devices.

He is currently involved with the Microwave Technology Center, Agilent Technologies, Santa Rosa, CA. He is also involved in the design, characterization, and optimization of millimeter-wave ICs used for high-performance instrumentation. His interests include reactively matched LNAs, broad-band power amplifiers, and traveling-wave amplifiers in both coplanar and microstrip topologies.